REPORT DOCUMENTATION PAGE

Form Approved
OMB No. 0704-0188

1. REPORT DATE *(DD-MM-YYYY)*	2. REPORT TYPE	3. DATES COVERED *(From - To)*
29-07-2014	Conference Proceeding	

4. TITLE AND SUBTITLE
The Impact of Turbulent Fluctuations on Light Propagation in a Controlled Environment

5a. CONTRACT NUMBER

5b. GRANT NUMBER

5c. PROGRAM ELEMENT NUMBER
0602782N

6. AUTHOR(S)
Silvia Matt, Weilin Hou and Wesley Goode

5d. PROJECT NUMBER

5e. TASK NUMBER

5f. WORK UNIT NUMBER
73-6604-04-5

7. PERFORMING ORGANIZATION NAME(S) AND ADDRESS(ES)
Naval Research Laboratory
Oceanography Division
Stennis Space Center, MS 39529-5004

8. PERFORMING ORGANIZATION REPORT NUMBER
NRL/PP/7330--14-2145

9. SPONSORING/MONITORING AGENCY NAME(S) AND ADDRESS(ES)
Office of Naval Research
One Liberty Center
875 North Randolph Street, Suite 1425
Arlington, VA 22203-1995

10. SPONSOR/MONITOR'S ACRONYM(S)
ONR

11. SPONSOR/MONITOR'S REPORT NUMBER(S)

12. DISTRIBUTION/AVAILABILITY STATEMENT
Approved for public release, distribution is unlimited.

13. SUPPLEMENTARY NOTES

14. ABSTRACT
Underwater temperature and salinity microstructure can lead to localized changes in the index of refraction and can be a limiting factor in oceanic environments. This optical turbulence can affect electro-optical (EO) signal transmissions that impact various applications, from diver visibility to active and passive remote sensing. To quantify the scope of the impacts from turbulent flows on EO signal transmission, and to examine and mitigate turbulence effects, we perform experiments in a controlled turbulence environment allowing the variation of turbulence intensity. This controlled turbulence setup is implemented at the Naval Research Laboratory Stennis Space Center (NRLSSC). Convective turbulence is generated in a classical Rayleigh-Benard tank and the turbulent flow is quantified using a state-of-the-art suite of sensors that includes high-resolution Acoustic Doppler Velocimeter profilers and fast thermistor probes. The measurements are complemented by very high-resolution non-hydrostatic numerical simulations. These computational fluid dynamics simulations allow for a more complete characterization of the convective flow in the laboratory tank than would be provided by measurements alone. Optical image degradation in the tank is assessed in relation to turbulence intensity. The unique approach of integrating optical techniques, turbulence measurements and numerical simulations helps advance our understanding of how to mitigate the effects of turbulence impacts on underwater optical signal transmission, as well as of the use of optical techniques to probe oceanic processes.

15. SUBJECT TERMS
optical turbulence, laboratory experiments, ADV profiler, TKED, TD

16. SECURITY CLASSIFICATION OF:			17. LIMITATION OF ABSTRACT	18. NUMBER OF PAGES	19a. NAME OF RESPONSIBLE PERSON
a. REPORT	b. ABSTRACT	c. THIS PAGE			Weilin Hou
Unclassified	Unclassified	Unclassified	UU	11	19b. TELEPHONE NUMBER *(Include area code)* (228) 688-5257

The impact of turbulent fluctuations on light propagation in a controlled environment

Silvia Matt [1], Weilin Hou [2], and Wesley Goode [2]

[1] National Research Council Postdoctoral Research Associate
[2] Ocean Sciences Branch, Naval Research Laboratory, Stennis Space Center, MS, USA

ABSTRACT

Underwater temperature and salinity microstructure can lead to localized changes in the index of refraction and can be a limiting factor in oceanic environments. This optical turbulence can affect electro-optical (EO) signal transmissions that impact various applications, from diver visibility to active and passive remote sensing. To quantify the scope of the impacts from turbulent flows on EO signal transmission, and to examine and mitigate turbulence effects, we perform experiments in a controlled turbulence environment allowing the variation of turbulence intensity. This controlled turbulence setup is implemented at the Naval Research Laboratory Stennis Space Center (NRLSSC). Convective turbulence is generated in a classical Rayleigh-Bénard tank and the turbulent flow is quantified using a state-of-the-art suite of sensors that includes high-resolution Acoustic Doppler Velocimeter profilers and fast thermistor probes. The measurements are complemented by very high-resolution non-hydrostatic numerical simulations. These computational fluid dynamics simulations allow for a more complete characterization of the convective flow in the laboratory tank than would be provided by measurements alone. Optical image degradation in the tank is assessed in relation to turbulence intensity. The unique approach of integrating optical techniques, turbulence measurements and numerical simulations helps advance our understanding of how to mitigate the effects of turbulence impacts on underwater optical signal transmission, as well as of the use of optical techniques to probe oceanic processes.

Keywords: optical turbulence, laboratory experiments, ADV profiler, TKED, TD

1. INTRODUCTION

Turbulent flows are an intergral part of the natural environment. In the ocean, the mixing that accompanies turbulent flows is an important part of the global energy budget and of localized water mass exchanges. Small-scale temperature and salinity variations, i.e. temperature and salinity microstructure, which are associated with turbulent mixing, can also lead to localized changes in the index of refraction, which may affect underwater optical properties. This phenomenon has been demonstrated to have the potential to be a limiting factor in oceanic environments, affecting optical signal transmissions that impact various naval and civilian applications, from diver visibility to active and passive remote sensing.[1]

To quantify the scope of the impacts from turbulent flows on optical signal transmission, and to better understand how to mitigate these impacts in the underwater environment, we implemented a controlled turbulence setup, where convective turbulence is generated in a classical Rayleigh-Bénard tank (dimensions are $5m$ by $0.5m$ by $0.5m$) (Fig. 1). The goal was to develop a setup where turbulence strength - convective turbulence in our case - can be adjusted, while also being characterized in terms of turbulent kinetic energy dissipation ϵ (TKED) and temperature variance dissipation rate χ (TD). This controlled turbulence environment can then serve as a testbed for optical methods to mitigate the effect of turbulence on EO signal transmission.

Corresponding author: Silvia Matt: E-mail: silvia.matt.ctr@nrlssc.navy.mil

Ocean Sensing and Monitoring VI, edited by Weilin W. Hou, Robert A. Arnone, Proc. of SPIE
Vol. 9111, 911113 · © 2014 SPIE · CCC code: 0277-786X/14/$18 · doi: 10.1117/12.2053062

Figure 1. Laboratory tank at NRLSSC. The photo on the right shows the Vectrino profiler ADV and the CT temperature probe.

2. METHODS

Convective turbulence was generated in the RB tank by heating a stainless steel plate at the bottom of the tank and cooling a similar plate at the top of the tank. The strength of the convective turbulence in the tank is a function of the temperature difference across the tank and can be characterized in terms of the Rayleigh number, defined as

$$Ra = \frac{g\alpha\Delta T d^3}{\nu D_T} \tag{1}$$

Here, g is the acceleration due to gravity, α is the thermal expansion coefficient, ΔT is the temperature difference between the plates, d is the distance between the plates, ν is the kinematic viscosity, and D_T is the thermal diffusivity. In our experiments, Ra ranges from $1.5 \cdot 10^{10}$ to around $4 \cdot 10^{10}$, corresponding to a temperature difference across the plates ΔT of $6K$ and $16K$, respectively (Table 1). Note that this temperature difference is the difference between the temperature on the plates proper, the temperature gradient that sets up in the interior of the tank is much less pronounced.

To characterize the turbulent environment in the RB tank, the turbulent flow is quantified by high-resolution Acoustic Doppler Velocimeter profilers (Nortek Vectrino Profiler) and fast thermistor probes (PME high-resolution conductivity-temperature (CT) probe) (Fig. 1, right). These instruments provide high-resolution velocity and temperature measurements, at 100 and $64Hz$ respectively. The ADV and CT probes were mounted in the RB tank and collected time series of high-resolution velocity and temperature/conductivity for the subsequent estimation of TKED and TD rates. Data were collected at a sampling frequency of $100Hz$ with the Vectrino Profiler and at $64Hz$ with the CT probe, which is controlled by the Nortek Vector ADV in our setup. A high-speed imaging camera and active optical target, an iPad displaying resolution patterns, were placed at opposite ends of the tank, providing an optical path length of around $5m$. This served the purpose of putting the turbulence data into the context of measurements of optical target clarity.

The turbulent kinetic energy dissipation (TKED) and temperature variance dissipation (TD) rates were calculated from the velocity and temperature measurements via spectral fitting to Kolmogorov spectra (for velocity) and Batchelor spectra (for temperature) and compared to values obtained from the numerical simulations of the RB tank for comparable Rayleigh number and setup (see Section 2.1).

2.0.1 Numerical Tank

The laboratory measurements were complemented by very high-resolution, non-hydrostatic numerical simulations. These simulations provide full fields of temperature and velocity for the estimation of turbulence parameters and their impact on the optics (Fig. 2).

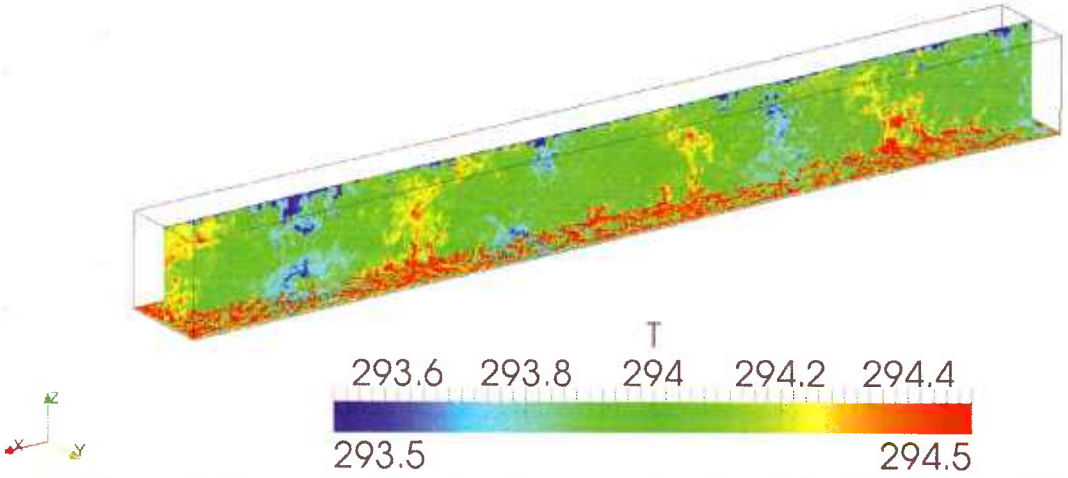

Figure 2. Example of the "Numerical Tank" used to simulate Rayleigh-Bénard convection and emulating the laboratory tank setup.

The numerical experiments (as listed in Table 1,) were performed with the open-source Computational Fluid Dynamics (CFD) package OpenFOAM. We use a Large-Eddy Simulation (LES) formulation, with the traditional Smagorinsky model as a sub-grid scale model. In LES, the larger-scale eddies in the flow are explicitely resolved, while the scales smaller than the grid-size are modeled. We run at two resolutions: a centimeter scale simulation with $\Delta x = \Delta y = \Delta z = 1cm$, which corresponds to 1.25 million grid points in the domain, and a very high-resolution, millimeter-scale simulation with $\Delta x = \Delta y = 5mm$, $\Delta z = 2.5mm$, which corresponds to 20 million grid points. The former can be run comfortably on a modern, high-performance, dual six-core Linux desktop, making use of all 12 cores, whereas the latter requires the use of a High-Performance Computing facility, due to the high computational cost. In our case, the code was run on 96 processors on one of the IBMs at the Navy DoD Supercomputing Resource Center.

At these resolutions, the flow is very well resolved, down to the Kolmogorov scales, and the contribution from the sub-grid scale model is small, especially in our very high-resolution run. In this paper, we show results from the millimeter-scale resolution run, unless otherwise noted.

We also explored cases with the numerical tank, where the temperature on the heating (cooling) plates was not uniform, but rather decreased (increased) towards the center of the tank. The plates in our laboratory setup are heated (cooled) by water flowing into the plates and these experiments helped us to more accurately assess the impact of heat loss over the plates on the convective turbulence in the interior. The main effect appeared to be that the reduced heat input lowered the Rayleigh number of the flow and thus reduced the strength of convection in the tank. To help quantify this result, and to compare simulations, we calculated the variance of temperature T and of vertical velocity w along a centerline at half-depth in the tank. These values are shown in Table 1.

2.1 Calculation of TKED and TD

2.1.1 Turbulent Kinetic Energy Dissipation rate - TKED

Spectra were calculated from either velocity sections (model) or from velocity time-series (laboratory data), in which case Taylor's Frozen Turbulence hypothesis (see, f. ex., Ref. 2), $k = \frac{2\pi f}{U}$, had to be applied to convert the frequency spectra to wavenumber spectra. Here, k is the wavenumber (in $rad\,m^{-1}$), f is the frequency (in s^{-1}), and U is the mean flow past the sensor (in $m\,s^{-1}$). The dominant velocity direction is vertical in our case, and we use the mean flow associated with the up/downdraft past the sensor. A wavenumber range respresentative of the spectrum in the ISR is chosen and the TKED rate ϵ is estimated from

Exp#:	1	2	3	4	5	6	7
Ra	$4 \cdot 10^{10}$	$4 \cdot 10^{10}$	$2 \cdot 10^{10}$	$1.5 \cdot 10^{10}$	$4 \cdot 10^{10}$	$4 \cdot 10^{10}$	$4 \cdot 10^{10}$
ΔT_{tank}	16	16	8	6	16 (14)	16 (12)	16 (8)
T_{bott}	302	302	298	297	302	302	302
T_{top}	286	286	290	291	286	286	286
ΔT_{plates}	no	no	no	no	$\pm(1°)$	$\pm(2°)$	$\pm(4°)$
var(w)	$3.6 \cdot 10^{-5}$	$2.4 \cdot 10^{-5}$	$1.1 \cdot 10^{-5}$	$1.2 \cdot 10^{-5}$	$2.1 \cdot 10^{-5}$	$2.3 \cdot 10^{-5}$	$1.9 \cdot 10^{-5}$
var(T)	0.0060	0.0040	0.0009	0.0007	0.0024	0.0014	0.0016
Resol.	$5x2.5mm$	$1cm$	$1cm$	$1cm$	$1cm$	$1cm$	$1cm$

Table 1. Table of numerical experiments.

$$E_{ii}(k_1) = C\epsilon^{\frac{2}{3}} k_1^{-\frac{5}{3}}, \tag{2}$$

where

$$\int_0^\infty E_{ii}(k_1)\, dk_1 = \bar{u}_i^2. \tag{3}$$

Here, E_{ii} is the one-dimensional velocity spectrum of component i ($x_1 = x$ is the streamwise component, $x_2 = y$ is the transverse component, and $x_3 = z$ is the vertical component, in a Cartesian coordinate system), and $\bar{u}_i^2$ is the variance of the signal. C is a constant equal to $\frac{18}{55}\,\alpha$ in the streamwise direction (x and k_1) and to $\frac{4}{3}\,\frac{18}{55}\,\alpha$ in the transverse or vertical direction (y, z) ; $\alpha \approx 1.5$ is the Kolmogorov constant (see, for example,[3]). Note that in our case, since we use the vertical velocity as the mean flow U, we need to make sure to use the appropriate C, i.e., $\frac{18}{55}\,\alpha$ for the vertical direction and $\frac{4}{3}\,\frac{18}{55}\,\alpha$ for the horizontal directions.

2.1.2 Temperature Dissipation rate - TD

For the estimation of TD rates from the temperature sections (model) or time series (laboratory), we calculated temperature gradient spectra and fit them to the theoretical Batchelor spectrum.[4] This technique involves fitting the temperature gradient spectra in the dissipative high-frequency range of the spectrum, which is poorly resolved and very noisy in the laboratory data. To obtain temperature gradient spectra from the temperature time series in the laboratory, we again invoke Taylor's frozen turbulence hypothesis and use

$$\frac{dT}{dx} = \frac{1}{U}\frac{dT}{dt} \tag{4}$$

and $\hat{k} = f/U$ (note that in this case, $\hat{k}$ has units of cpm) . For isotropic turbulence, the dissipation rate of the temperature variance can be described as

$$\chi_T = 6D_T\langle\frac{dT}{dx}\frac{dT}{dx}\rangle = 6D_T\int_0^\infty \Psi_{T_x}(k)\, dk, \tag{5}$$

where D_T is the thermal diffusivity, and $\Psi_{T_x}(k)$ is the wavenumber spectrum of $\frac{dT}{dx}$, the alongpath component of the temperature gradient.[5] To ensure that U varies as little as possible over the segment used to calculate temperature gradient spectra, the laboratory spectral estimates were done from 1-second data segments and the results for χ were averaged.

We explored the use of the Maximum Likelihood Estimator technique (MLE) of spectral fitting to our data,[4] which works very well for the wavenumber spectra directly calculated from model data, without the use of the frozen turbulence hypothesis. In the case of the laboratory data, our spectra do not well resolve the high-frequency part of the spectrum, up to the Batchelor cut-off wavenumber k_B, and we instead chose to integrate the theoretical spectrum, according to.[5]

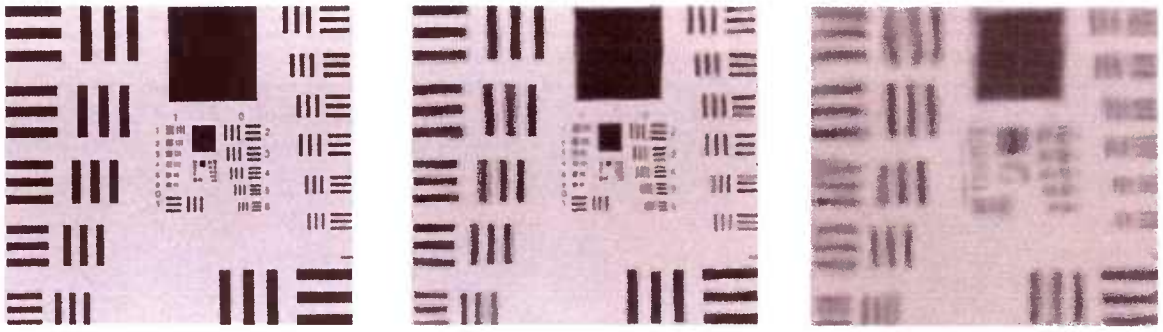

Figure 3. Image degradation for different optical turbulence strength.

2.2 Optical Turbulence

As noted previously, the turbulence data was collected in the context of optical target clarity and spatial resolution. High-definition video of an optical chart across the tank was taken during experiments and the images assessed for image degradation. The optical chart used was an image on an iPad screen, the camera was a Casio EXILIM EX-F1, and the videos were shot in High-Definition (HD), with $30fps$ and resolution 1920 by 1080 pixels. Note that the ADVs require seeding of the water in the tank to collect meaningful velocity data, which affects the water clarity. Hence, the videos shown here were taken immediately preceeding the seeding of the water, but after the tank had reached a steady-state with respect to convective turbulence.

Images from the laboratory show the image degradation due to optical turbulence for a case of strong (Fig. 3, center, $\Delta T \sim 6K$) and extreme optical turbulence (Fig. 3, right, $\Delta T \sim 16K$). Here, particle scattering is secondary to the changes in the index of refraction (IOR) due to temperature microstructure. Note that the effect of optical turbulence is more pronounced at the higher spatial frequencies. To quantify the extent of image degradation from optical turbulence, we apply the Structural Similarity Index Method (SSIM).[6] The SSIM is an image quality metric and measures the similarity between two images, when one is considered the "perfect quality" reference image (Fig. 3, left).

3. RESULTS

3.1 Image degradation

Results from applying the SSIM metric to the images collected at the different turbulence strengths shown in Figure 3, show increased degradation for stronger optical turbulence, i.e., higher Rayleigh number (Fig. 4) .

3.2 Model Temperature Variations and Circulation

To characterize the turbulence in the tank that is associated with the image degradation shown in Figure 4, we analyze the results from the laboratory measurements and the numerical tank. In the case of the numerical experiments, we want to make sure that the model has reached a steady-state and that the convective flow is fully developed. To investigate this time evolution of the convective turbulence in the domain, we look at a time series of the average value of the variance along a spatial section taken from the center line of the tank, for both temperature and vertical velocity. The results show that the model reaches a steady-state after about $15 - 20$ minutes (Fig. 5, data shown are from the cm-scale resolution run). The variability after this time can be attributed to the dynamics of convective cells and the circulation in the tank.

These convective cells are also apparent in temperature and velocity fields from the model (along the section shown in Fig. 2) and show the convective cells that develop in the tank (Fig. 6). The size of these convective cells is governed by the height of the tank, and we count about four to five up- and downdrafts. The index of refraction (IOR) in the tank can be calculated from the temperature fields[7] and also shows variability associated with the convective cells in the tank. Successive cross-sections of temperature taken halfway along the tank (at $x = 2.5m$) also illustrate the circulation (Fig. 7) and variability associated with this dynamic system. While

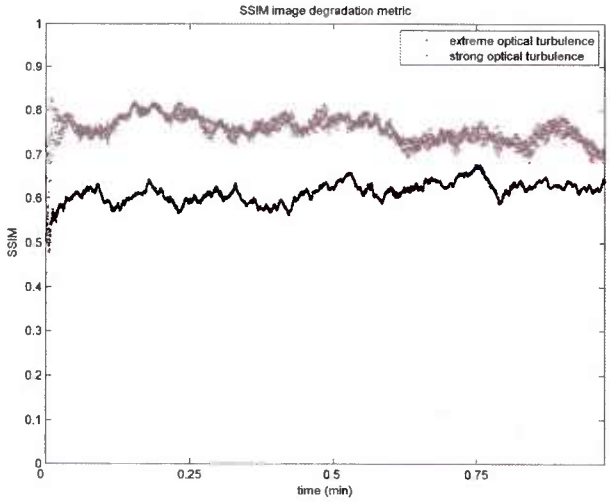

Figure 4. Image degradation for different (optical) turbulence strength as shown in Fig. 3 quantified by applying the SSIM method.

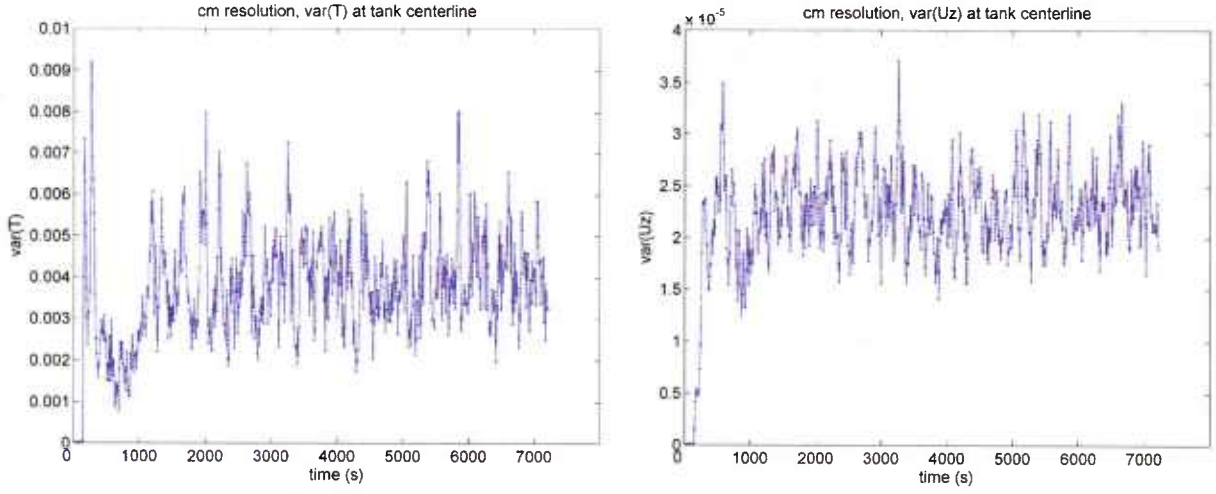

Figure 5. Time series of variance in the model from cm-scale resolution run.

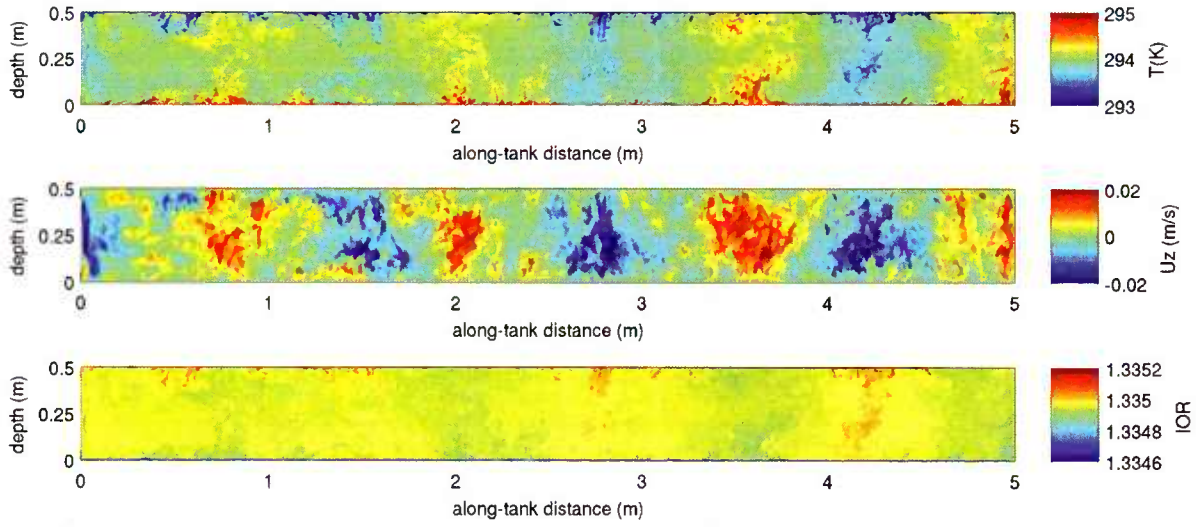

Figure 6. Model results at time t = 1050s, showing a sideview of temperature T (top), vertical velocity (Uz) (middle) and the Index of Refraction (IOR) calculated from the temperature field (bottom). The data is shown on the center plane of the tank.

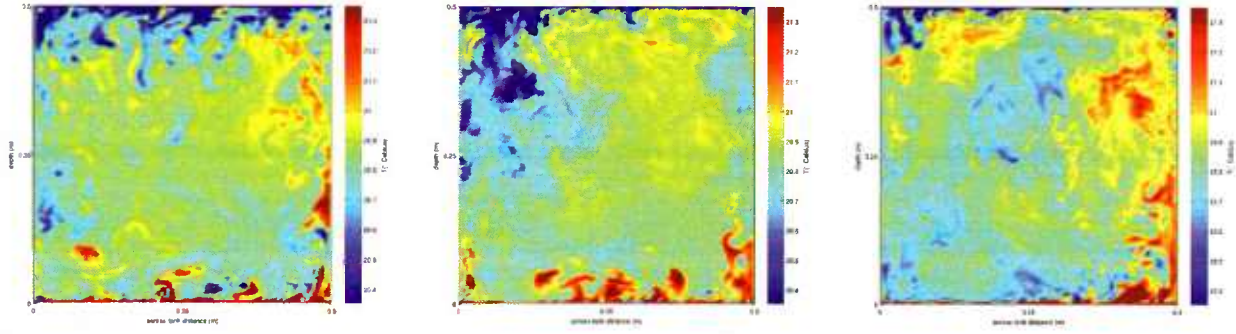

Figure 7. Snap shots of a tank cross section of temperature (in $^{\circ}C$) illustrate the variability associated with the convective cells and the dynamic environment in the tank ($x = 2.5m$; at times $t = 850s$, $875s$ and $950s$, from left to right).

the velocities associated with the flow are small ($O(2cm/s)$, the overturning still appears vigorous when we look at the temperature microstructure. The cross-sectional circulation is also apparent when looking at streamlines from the simulation. Figure 8 shows the updraft on one side of the tank near the center and downdrafts on the opposing side.

We can again calculate the IOR from the model temperature fields, and the cross-sections shown in Fig. 9 (top) mirror the variability seen in the temperature. To assess the effect on an optical beam across the tank, which experiences the cumulative effect of the turbulent variations in its path, we averaged the IOR at each point in the y-z plane over the entire length of the tank. As can be expected from the averaging procedure, this notably reduces the variability seen in the cross-sections. Since the beam passes through different layers of turbulence along its path, each of which varies in time and space, averaging of the fields may not be the appropriate approach to estimate the extent of beam distortion due to cumulative changes in IOR. Rather, a more involved approach directly tracing the beam's path through the medium may need to be adopted in future work.

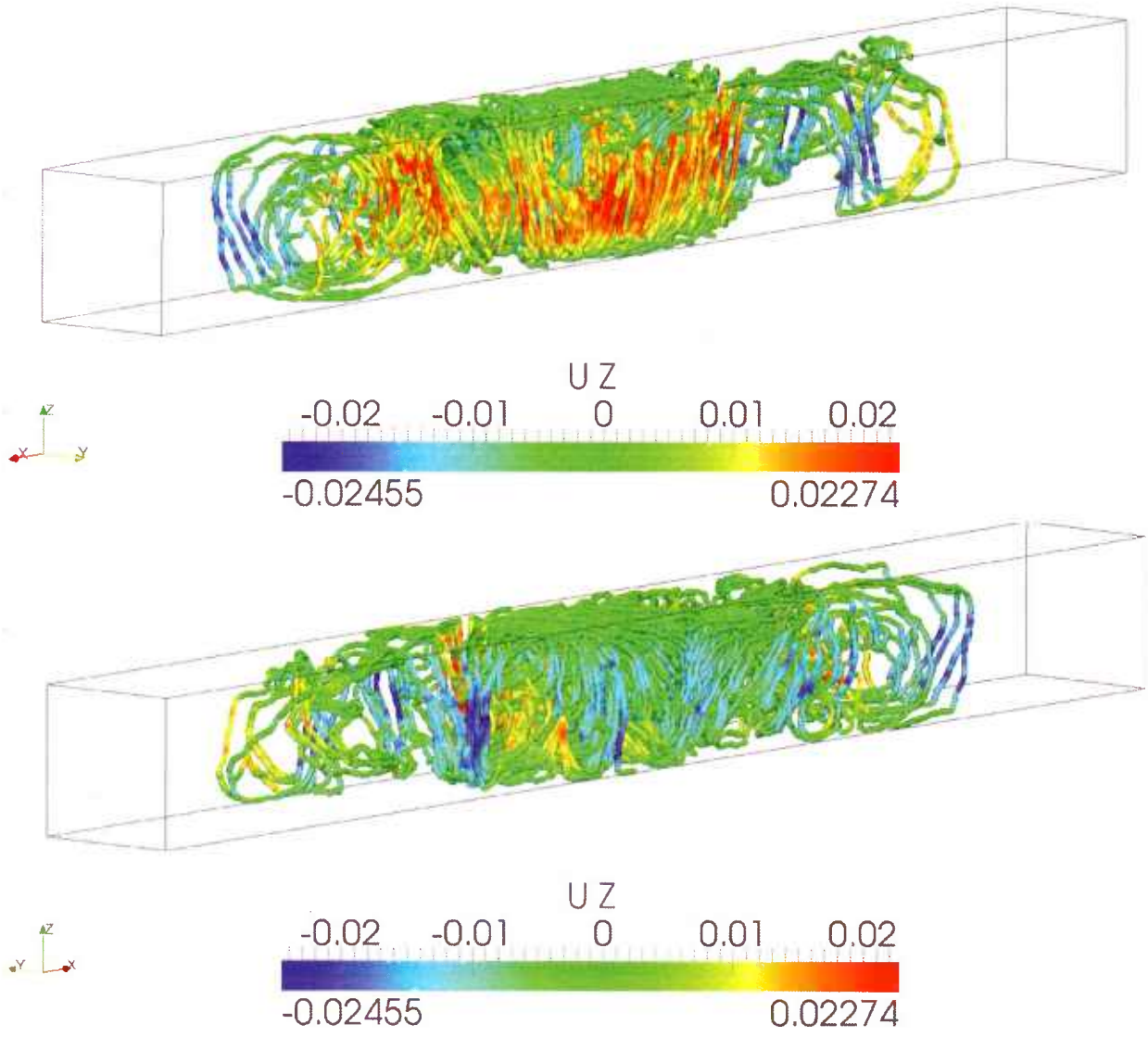

Figure 8. Model results at time $t = 1050s$, showing streamlines in the domain colored by vertical velocity Uz (top). The bottom plot shows the same but looking at it from the other side of the tank (x- and y-axis reversed). The updrafts and downdrafts illustrate that there is a circulation in the tank in the cross-sectional direction.

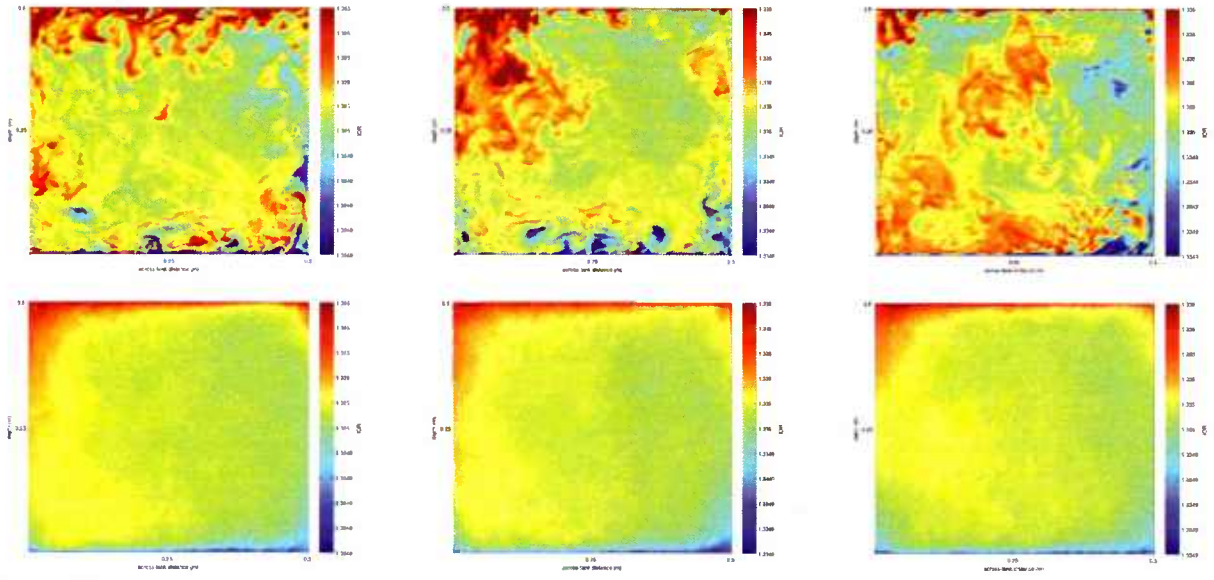

Figure 9. Top: The IOR calculated from the snap shots of the tank cross section of temperature shown in Fig. 7 illustrate the variability in terms of IOR. Bottom: Since an optical beam across the tank experiences the cumulative effect of the turbulent variations in its path, we averaged the IOR at each point in the y-z plane over the entire length of the tank. As can be expected, the averaging notably reduces the variability seen (at times $t = 850s$, $875s$ and $950s$, from left to right).

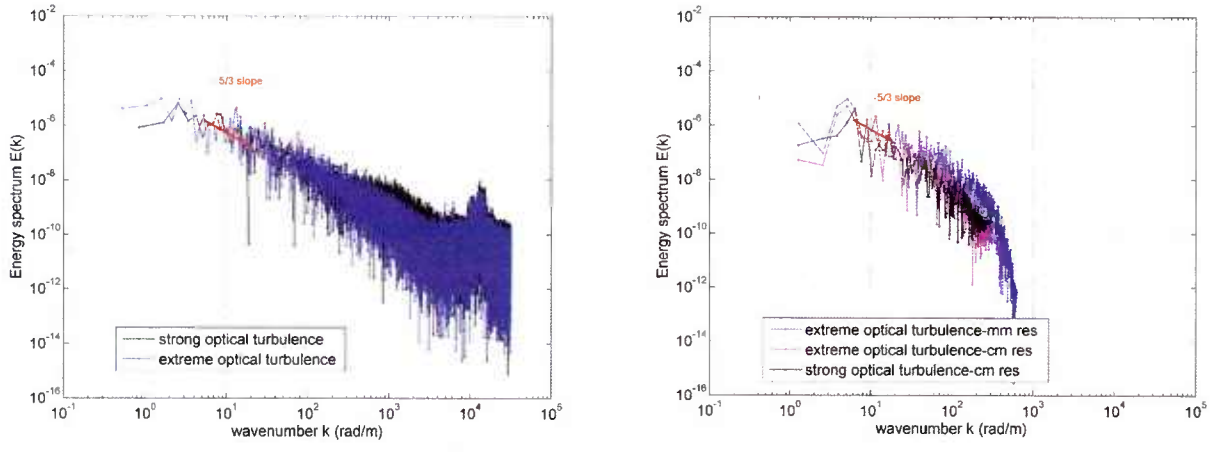

Figure 10. Energy spectra.

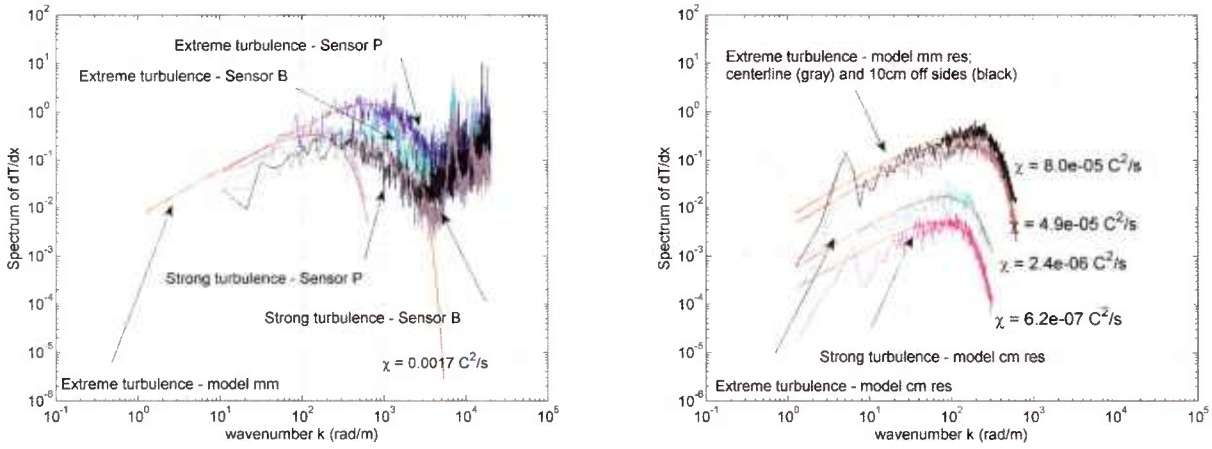

Figure 11. Temperature gradient spectra.

3.3 Spectra - Laboratory and Model

As described in Section 2.1, we calculate TKED and TD rates from both laboratory experiment and model to characterize the convective turbulence in the tank. Energy spectra $E(k)$ comparing lab (Fig. 10, left) and model (Fig. 10, right) show that the numerical model (especially at mm-scale resolution) adequately captures the turbulence spectrum in the inertial subrange and allows for the estimation of the TKED rates ϵ, which are of $O(10^{-7}W/kg)$ for the experiments shown.

The energy spectra do not show a significant difference in TKED between the experiments with different turbulence strength. As expected, the model energy spectra show a drop-off at the higher wavenumbers towards the dissipative range, which is resolution dependent.

While the model energy spectra accurately capture the inertial subrange, at levels comparable to the laboratory, the temperature gradient spectra show that the model (Fig. 11, right, as well as faint blue on left) has more difficulty reproducing the temperature gradients correctly. It is these temperature gradients, which are predominantly needed to assess optical turbulence The spectra illustrate that for different optical turbulence strengths, while the mechanical turbulence is comparable, the temperature gradient fields show a marked difference. Optical turbulence is mainly due to temperature variations affecting the IOR of water, and to adequately describe the effect on the optics, it is critical to resolve the temperature gradients. The value of χ (which was calculated following Ref. 4) is also strongly dependent on model resolution. The contribution of the sub-grid scale temperature fluctuations needs to be estimated to directly compare the temperature gradient spectra between model and laboratory. Estimating the model sub-grid scale contribution to χ and eliminating potential errors associated with the use of Taylor's Frozen Turbulence hypothesis for the calculation of χ (and ϵ) from the laboratory data, are the subject of ongoing work.

4. SUMMARY AND DISCUSSION

In order to study the impact of temperature microstructure on underwater optical signal transmission, we performed experiments in a controlled laboratory environment complemented by high-resolution, non-hydrostatic numerical simulations. The goal was to develop a setup where turbulence levels can be controlled and fully characterized. This setup, which allows for repeatable experiments under controlled conditions, can help understand processes involved in optical turbulence and provide a platform for the testing of optical techniques to mitigate turbulence effects underwater. Optical turbulence is mainly due to temperature (or salinity) variations affecting the IOR of water, and to adequately describe the effect on the optics, it is particularly critical to resolve the temperature gradients. This can present a challenge in both the laboratory and the model, due to noise and resolution requirements, respectively. Further work is needed to adress questions related to sub-grid contributions in LES to the rate of temperature variance dissipation.

ACKNOWLEDGMENTS

We thank Danielle Wain, Cynthia Bluteau and Barry Ruddick for sharing their data processing routines. Sarah Woods contributed to the tank design and early instrumental setup. We are grateful to Joe Calantoni for allowing us the use of his Vectrino II instrument. This project was supported by ONR/NRL 73-6604. Silvia Matt is supported by a National Research Council (NRC) Research Associateship.

REFERENCES

[1] Hou, W., Woods, S., Jarosz, E., Goode, W., and Weidemann, A., "Optical turbulence on underwater image degradation in natural environments," *Appl. Opt* **51**(15), 2678–2686 (2012).

[2] Tennekes, H. and Lumley, J. L., [*A first course in turbulence*], MIT Press (1972).

[3] Rusello, P. and Cowen, E., "Turbulent dissipation estimates from pulse coherent doppler instruments," in [*Current, Waves and Turbulence Measurements (CWTM), 2011 IEEE/OES 10th*], 167–172 (2011).

[4] Ruddick, B., Anis, A., and Thompson, K., "Maximum likelihood spectral fitting: The batchelor spectrum," *J. Atmos. Oceanic Technol.* **17**, 1541–1555 (2000).

[5] Moum, J. and Nash, J., "Mixing measurements on an equatorial ocean mooring," *J. Atmos. Oceanic Technol.* **26**, 317–336 (2009).

[6] Wang, Z., Bovik, A. C., Sheikh, H. R., and Simoncelli, E. P., "Image quality assessment: From error visibility to structural similarity," *IEEE Transactions on Image Processing* **13**, 600–612 (2004).

[7] Quan, X. and Fry, E. S., "Empirical equation for the index of refraction of seawater," *Applied Optics* **34**, 3477–3480 (1995).